recycling

MDPI

Article

Performance Constraints on Recycling Waste Tyre Carbon Black as a Cement Replacement in Masonry Mortars

Anghelo Manuel Torres-Vásquez, Denys Agustin Pacheco-Torres, Jorge Luis Leiva-Piedra *, Higeiny Adubel Aguinaga-Ramírez and Walter Manuel Hoyos-Alayo

Research Department, Faculty of Engineering, Universidad Tecnológica del Perú, Chiclayo 14011, Peru; 1637695@utp.edu.pe (A.M.T.-V.); u17103747@utp.edu.pe (D.A.P.-T.); c26247@utp.edu.pe (H.A.A.-R.); c23712@utp.edu.pe (W.M.H.-A.)
* Correspondence: jleiva@utp.edu.pe

Abstract

Recycling tyre-pyrolysis carbon as a cement substitute requires assessment of both bulk mortar and masonry interfaces. This study examined waste tyre carbon black (WTCB) at 0, 2.5, 5.0 and 7.5% cement replacement by mass without dispersing admixtures. Sand and effective water remained constant, with an effective water-to-total-powder ratio of 0.63. We measured fresh mortar flow and tested 180 specimens for mortar compression, direct tension, flexure, masonry prism compression, nominal diagonal shear and mortar–unit bond. Flow decreased from 113.06% to 105.94%. At 28 days, the 5.0% mixture had the highest mean mortar compressive strength (13.364 MPa), whereas the 7.5% mixture had the highest mean direct tensile strength (2.038 MPa). The 2.5% mixture had the highest mean prism strength on both test dates and the highest mean nominal diagonal shear strength at 28 days. It also showed the largest bond loss. At 28 days, all modified mixtures had lower flexural and bond means than the control, with bond losses of 17.5–46.2%. These differing rankings identify mortar–unit bond as an additional criterion for evaluating WTCB cement replacement alongside bulk strength. The results support further qualification of low replacement levels in the tested mortar–unit system.

Keywords: end-of-life tyres; waste valorisation; pyrolysis carbon; secondary raw materials; cement replacement; masonry mortar; bond strength

1. Introduction

Recycling residues into construction products requires both a destination for the secondary material and retention of the function supplied by the displaced constituent. For tyre-pyrolysis carbon, cement substitution offers a route into mineral products, but the useful replacement level depends on mortar and masonry performance. The International Energy Agency identifies material efficiency and alternative cement constituents among the measures supporting cement-sector decarbonisation [1]. Carbonaceous powders differ from conventional supplementary cementitious materials because their contribution depends on particle characteristics, dispersion and cement displacement rather than an assumed pozzolanic reaction.

End-of-life tyres provide one source of carbonaceous material. Peru established a specific framework for their management through Decreto Supremo N.° 024-2021-MINAM [2]. Pyrolysis produces a carbon-rich solid containing residues inherited from tyre formulations and processing. Rikmann et al. showed that mineral and organic impurities influence

Check for updates

Academic Editor: Sha Liang

Received: 21 October 2026
Revised: 23 November 2026
Accepted: 24 November 2026
Published: 27 November 2026

Copyright: © 2026 by the authors. Licensee MDPI, Basel, Switzerland. This article is an open access article distributed under the terms and conditions of the Creative Commons Attribution (CC BY) license.

the surface properties and processing of this material [3]. Here, waste tyre carbon black (WTCB) denotes the supplied pyrolysis-derived carbonaceous solid. Its source composition and preparation route distinguish it from commercial carbon black grades.

Published results also depend on how the carbon is introduced. Abdulfattah et al. investigated pyrolysed carbon black as an additive in concrete while maintaining the cement content and incorporating a superplasticiser [4]. Sabrin et al. examined pyrolysis carbon black as a cement replacement in mortar at 5–20%, providing a closer comparison with binder substitution [5]. Zhao et al. instead evaluated recovered carbon black from off-the-road tyres as an aggregate constituent for thermal-insulation mortar [6]. These approaches change different parts of the mixture, so their preferred dosages cannot be transferred directly to masonry mortar.

Carbonaceous particles can alter water demand and hydration when their surface chemistry and dispersion are controlled. Brial et al. used thermal analysis to examine how low replacement levels of several carbonaceous materials affected hydration [7]. Zhang et al. showed that sodium dodecyl sulphate modified the dispersion and performance of nano-carbon-black cement paste [8], while de Lima et al. linked carbon black nanoparticle content to hydration, void structure and mechanical response in mortar containing a polycarboxylate superplasticiser [9]. Karthikeyan and Elavenil reported agglomeration at higher carbon contents in silica-fume mortars even after ultrasonication and the addition of a superplasticiser [10]. These studies provide mechanistic hypotheses for examining WTCB mixtures prepared without dispersing admixtures.

Previous studies establish that tyre-derived carbon can alter cementitious properties, but their dosage rankings depend on whether the carbon replaces cement, supplements cement or replaces aggregate. The unresolved application question is whether a favourable bulk mortar response also preserves the mortar–unit interface and masonry assemblage behaviour. Prism, panel and bond responses depend on the constituent materials and their interaction [11,12]. We therefore compared 0, 2.5, 5.0 and 7.5% WTCB cement replacement across flow and six mechanical responses. The contribution is the identification of conflicting dosage rankings within one material system: a mixture with favourable prism and nominal diagonal shear means can simultaneously incur the greatest bond loss. This provides a functional criterion for recycling assessment beyond maximising waste content or mortar compressive strength.

2. Results

2.1. Fresh-State Flow

Flow decreased with WTCB replacement (Table 1), from 113.06% for the control to 111.03%, 107.23% and 105.94% at 2.5%, 5.0% and 7.5%, respectively. The maximum reduction was 7.13 percentage points, or 6.30% relative to the control.

Table 1. Fresh mortar flow at each nominal WTCB replacement.

WTCB (%)	Mean Spread D (mm)	Initial Diameter D_0 (mm)	Flow (%)
0.0	209.25	98.21	113.06
2.5	207.25	98.21	111.03
5.0	203.53	98.21	107.23
7.5	202.25	98.21	105.94

Flow = $100(D - D_0)/D_0$, where D is the mean of four directional diameters within one spread test. At 5.0% WTCB, the four readings give D = 203.525 mm and flow = 107.23% (Table S12). Displayed D values are rounded to two decimals.

2.2. Mortar Compressive Strength

Compressive strength increased with curing age at every dosage (Table 2 and Figure 1). The 28-day means were 12.601 MPa for the control, 12.432 MPa at 2.5%, 13.364 MPa at 5.0% and 12.295 MPa at 7.5%. The 5.0% mixture had the highest mean, 6.05% above the control, despite having the lowest means at 7 and 14 days. This descriptive ranking uses the individual loaded areas documented in Table S8 and Section 4.4.

Table 2. Mortar strengths calculated from individual recorded values.

Age (Days)	WTCB (%)	Compression (MPa)	Direct Tension (MPa)	Flexure (MPa)
7	0.0	9.671 ± 0.203	0.854 ± 0.106	3.147 ± 0.421
7	2.5	8.629 ± 0.391	0.988 ± 0.085	3.654 ± 0.375
7	5.0	8.187 ± 0.476	0.967 ± 0.042	2.940 ± 0.212
7	7.5	8.570 ± 0.504	0.948 ± 0.051	4.292 ± 0.199
14	0.0	10.410 ± 0.850	1.152 ± 0.034	6.619 ± 0.464
14	2.5	10.973 ± 0.230	1.444 ± 0.049	4.838 ± 0.300
14	5.0	9.240 ± 0.338	1.178 ± 0.075	5.620 ± 0.492
14	7.5	10.170 ± 0.926	1.672 ± 0.095	5.907 ± 0.272
28	0.0	12.601 ± 1.446	1.593 ± 0.198	7.132 ± 0.524
28	2.5	12.432 ± 0.993	1.618 ± 0.046	6.600 ± 0.370
28	5.0	13.364 ± 0.326	1.454 ± 0.004	6.942 ± 0.270
28	7.5	12.295 ± 1.090	2.038 ± 0.093	6.727 ± 0.530

Values are mean ± sample standard deviation ($n = 3$ specimens per dosage–age cell). Tension denotes direct briquette tension under NTP 334.060:2019. Original individual records appear in Tables S1–S3. Flexural summaries use the central-load recalculation documented in Tables S3 and S13.

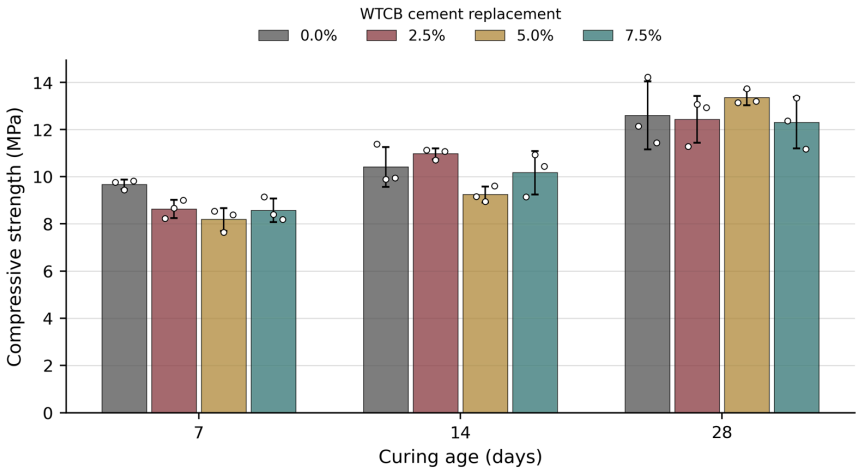

Figure 1. Mortar compressive strength by age and WTCB cement replacement. Bars show means, error bars show sample standard deviations, and points show individual specimens ($n = 3$ per dosage–age cell).

The compression model showed an association with curing age ($F_{2,24} = 82.891$, $p = 1.673 \times 10^{-11}$). The dosage term ($F_{3,24} = 1.371$, $p = 0.275$) and dosage–age interaction ($F_{6,24} = 2.370$, $p = 0.061$) did not reach the nominal threshold. Figures S1–S3 display specimen distributions and dosage–age summaries.

2.3. Direct Tensile Strength

At 28 days, the direct tensile means were 1.593 MPa for the control, 1.618 MPa at 2.5%, 1.454 MPa at 5.0% and 2.038 MPa at 7.5% (Table 2 and Figure 2). The 7.5% mixture exceeded the control mean by 27.94%, while the 5.0% mean was 8.72% lower.

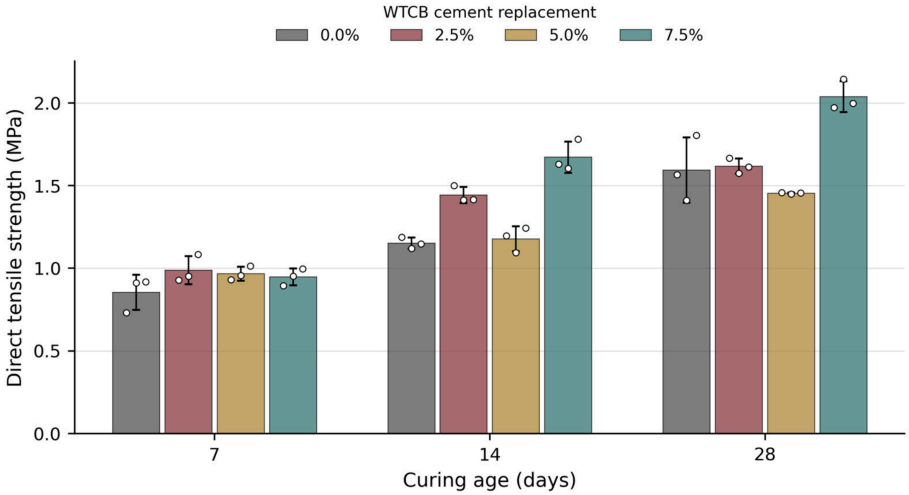

Figure 2. Mortar direct tensile strength by age and WTCB cement replacement. Bars show means, error bars show sample standard deviations, and points show individual briquettes ($n = 3$ per dosage–age cell).

The tensile model showed associations with dosage ($F_{3,24} = 33.212$, $p = 1.045 \times 10^{-8}$), age ($F_{2,24} = 216.596$, $p = 4.379 \times 10^{-16}$) and their interaction ($F_{6,24} = 8.598$, $p = 4.779 \times 10^{-5}$). The response varied across both dosage and curing time. For the 12 group means, Pearson r was 0.829 with age and 0.290 with dosage. Figures S4–S6 display the specimen distributions and these dosage–age summaries.

2.4. Flexural Strength

The control achieved the highest mean flexural strength at 28 days, 7.132 MPa (Table 2 and Figure 3). The means for the WTCB mixtures were 6.600, 6.942 and 6.727 MPa at 2.5%, 5.0% and 7.5%, corresponding to reductions of 7.46%, 2.67% and 5.68%, respectively. The 5.0% result was closest to the control. The 7.5% mixture had the highest mean at 7 days, whereas the control had the highest mean at 14 and 28 days.

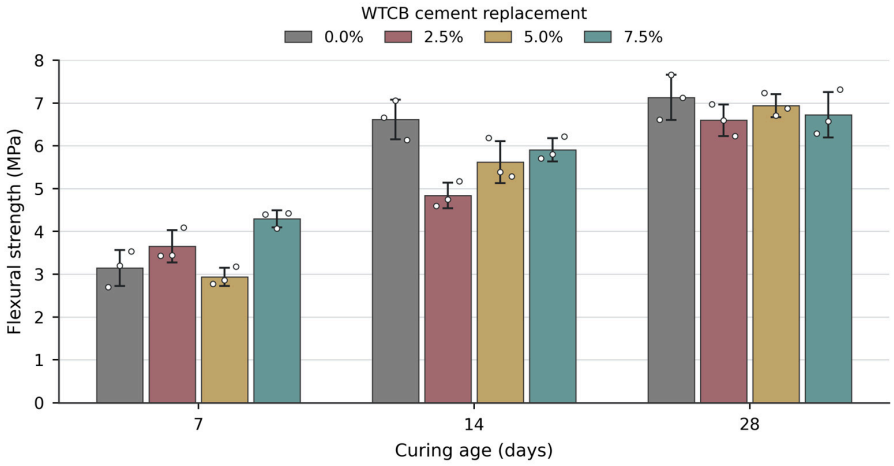

Figure 3. Mortar flexural strength by age and WTCB cement replacement. Bars show means, error bars show sample standard deviations, and points show individual beams ($n = 3$ per dosage–age cell).

Dosage ($F_{3,24} = 6.023$, $p = 0.003292$), age ($F_{2,24} = 233.346$, $p = 1.874 \times 10^{-16}$) and their interaction ($F_{6,24} = 6.661$, $p = 0.0003031$) met the nominal threshold for flexural strength. The interaction is consistent with the changing dosage ranking across ages. Figures S7–S9 show the specimen distributions, group-mean correlations and observed-mean grid.

2.5. Masonry Prism Compression

Across the two test dates, mean prism strengths were 5.598 MPa for the control, 7.125 MPa at 2.5%, 5.789 MPa at 5.0% and 4.855 MPa at 7.5% (Table 3 and Figure 4). The 2.5% group also had the highest mean on each date. Its mean was 6.035 MPa on 5 October and 8.215 MPa on 19 October, compared with 5.026 and 6.171 MPa for the controls tested on the same dates (Table S16).

Table 3. Masonry prism compressive strengths pooled over 5 and 19 October 2024. Individual curing ages were not recorded.

WTCB (%)	*n*	Prism Strength (MPa)	Change from Control (%)
0.0	6	5.598 ± 0.681	+0.00
2.5	6	7.125 ± 1.277	+27.27
5.0	6	5.789 ± 0.826	+3.41
7.5	6	4.855 ± 0.708	−13.27

Values are mean ± sample standard deviation for six prisms per dosage, three per test date. Strengths include the laboratory correction factor of 1.04 for the nominal height-to-thickness ratio of 2.5. Percentage differences refer to the pooled control mean. Table S16 gives the date-specific results.

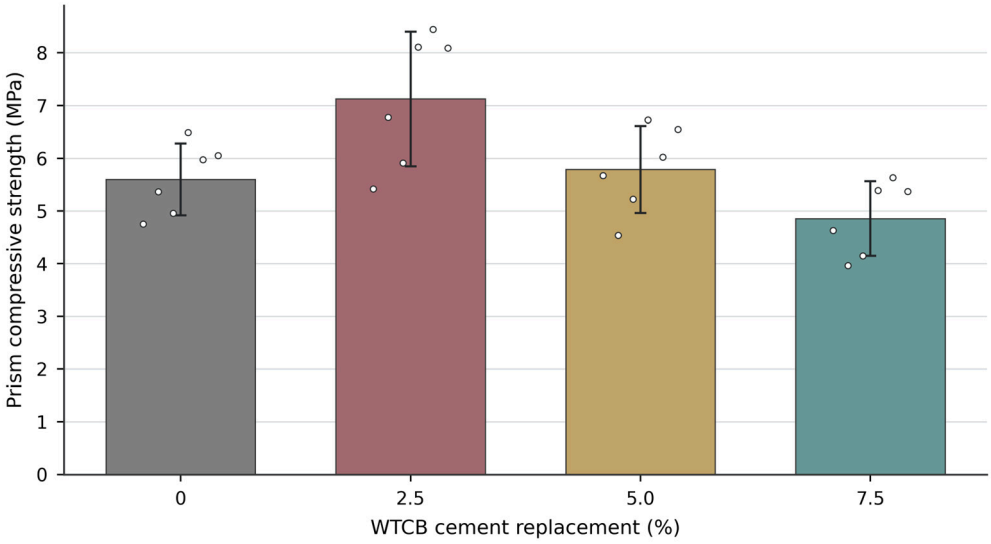

Figure 4. Masonry prism compressive strength pooled over 5 and 19 October 2024. Individual curing ages were not recorded. Bars show dosage means, error bars show sample standard deviations, and points show individual prisms ($n = 6$ per dosage). Grey, rose, ochre and teal bars indicate 0%, 2.5%, 5.0% and 7.5% WTCB replacement, respectively.

The pooled prism comparison gave $F_{3,20} = 6.545$ and $p = 0.00291$ for dosage. The 2.5% group had the largest sample standard deviation, 1.277 MPa.

2.6. Nominal Diagonal Shear Strength

All dosages showed higher mean nominal diagonal shear strength at 28 than at 14 days (Table 4 and Figure 5). At 28 days, the 2.5% group reached 0.937 MPa, 3.80% above the control mean of 0.902 MPa. The 5.0% and 7.5% means were 0.836 and 0.754 MPa, respectively. The mean declined as replacement increased from 2.5% to 7.5%.

Dosage ($F_{3,16} = 37.119$, $p = 1.953 \times 10^{-7}$) and age ($F_{1,16} = 94.812$, $p = 3.974 \times 10^{-8}$) met the nominal significance threshold, but their interaction did not ($F_{3,16} = 2.998$, $p = 0.0616$).

Supplementary Figures S10–S12 show the distributions, observed-mean grid and group-mean correlations.

Table 4. Nominal diagonal shear and direct tensile mortar–unit bond strengths.

Age (Days)	WTCB (%)	Nominal Diagonal Shear (MPa)	Bond (MPa)
14	0.0	0.830 ± 0.066	0.158 ± 0.017
14	2.5	0.771 ± 0.042	0.076 ± 0.001
14	5.0	0.646 ± 0.044	0.103 ± 0.004
14	7.5	0.610 ± 0.018	0.092 ± 0.003
28	0.0	0.902 ± 0.013	0.213 ± 0.024
28	2.5	0.937 ± 0.018	0.114 ± 0.007
28	5.0	0.836 ± 0.027	0.143 ± 0.011
28	7.5	0.754 ± 0.027	0.176 ± 0.007

Values are mean ± sample standard deviation ($n = 3$ per cell). Original specimen values appear in Tables S5 and S6.

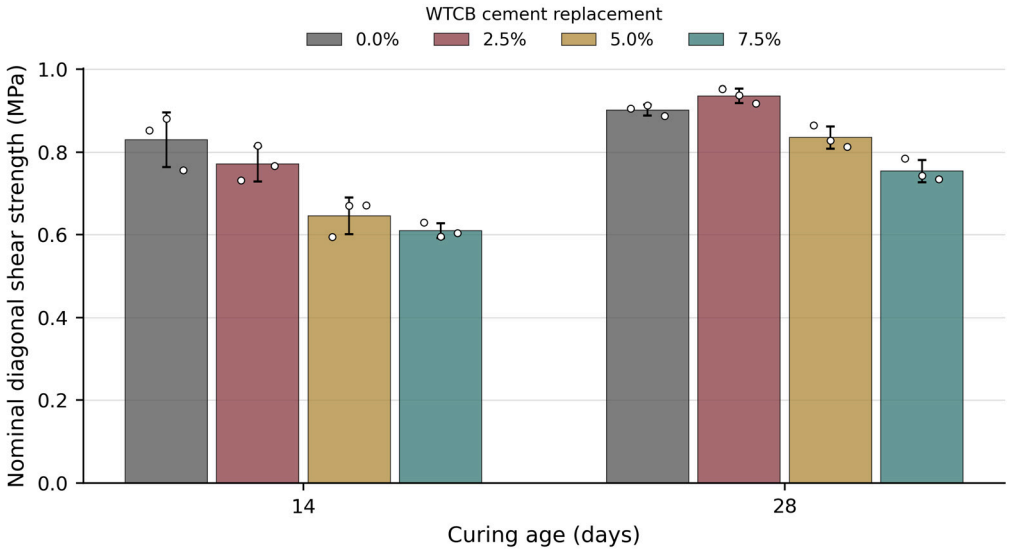

Figure 5. Nominal diagonal shear strength by age and WTCB cement replacement. Bars show means, error bars show sample standard deviations, and points show individual panels ($n = 3$ per dosage–age cell).

2.7. Mortar–Unit Bond

Bond strength increased with curing time for every dosage, but all WTCB mixtures remained below the control at both ages (Table 4 and Figure 6). The 28-day control mean was 0.213 MPa, compared with 0.114 MPa at 2.5%, 0.143 MPa at 5.0% and 0.176 MPa at 7.5%. The corresponding decreases were 46.24%, 32.72% and 17.51%, respectively. The 2.5% dosage thus combined the highest 28-day nominal diagonal shear mean with the largest bond loss.

The bond model showed associations with dosage ($F_{3,16} = 61.875$, $p = 5.061 \times 10^{-9}$), age ($F_{1,16} = 128.381$, $p = 4.705 \times 10^{-9}$) and their interaction ($F_{3,16} = 4.591$, $p = 0.0168$). The interaction is consistent with differences in bond development with curing. Supplementary Figures S13–S15 show the specimen distributions and group-mean summaries.

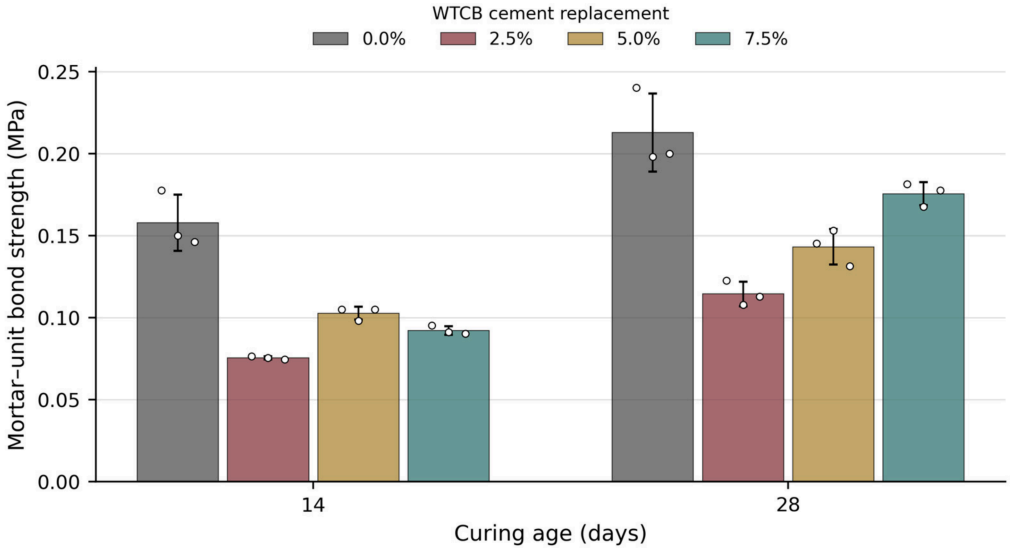

Figure 6. Mortar–unit direct tensile bond strength by age and WTCB cement replacement. Bars show means, error bars show sample standard deviations, and points show individual assemblies ($n = 3$ per dosage–age cell).

2.8. Comparison Across Performance Criteria

Table 5 compares each mixture with its control at 28 days for the age-labelled tests and across the two test dates for prisms. No modified dosage improved every response. The 2.5% mixture combined the smallest flow reduction among modified mixtures with the highest prism and nominal diagonal shear means, but its bond reduction was the largest. The 5.0% mixture produced the highest mortar compression mean and the closest flexural mean to the control. The 7.5% mixture gave the highest direct tensile mean and the smallest bond loss among the modified mixtures but lower flexural, prism and nominal diagonal shear means than the control. Table S9 reports the corresponding absolute mean differences and conditional uncertainty intervals.

Table 5. Relative changes in strength compared with the control.

Response	2.5% WTCB	5.0% WTCB	7.5% WTCB
Compression	−1.34	+6.05	−2.43
Direct tension	+1.56	−8.72	+27.94
Flexure	−7.46	−2.67	−5.68
Prism compression	+27.27	+3.41	−13.27
Nominal diagonal shear	+3.80	−7.39	−16.41
Mortar–unit bond	−46.24	−32.72	−17.51

Percentage differences use the unrounded means. Prism comparisons pool three specimens per dosage on each of the two test dates. All other rows compare the 28-day means. Positive values indicate a higher mean than the control.

Table 6 compares the role of the carbon across studies. Sabrin et al. [5] evaluated 5–20% cement replacement and selected 5% on cost and strength-to-CO_2 criteria. In our masonry tests, the mixture with the highest mean prism strength, at 2.5% replacement, also had the largest loss of mortar–unit bond strength. The preferred dosage therefore depends on the performance criterion.

Table 6. Comparison of tyre-derived carbon roles and the contribution of the present programme.

Study	Carbon Role and Dosage	Preparation or Dispersion	Relevance to This Study
Abdulfattah et al. [4]	Tyre-pyrolysis carbon added to concrete at fixed cement content	Superplasticiser incorporated	Addition does not quantify cement displacement.
Sabrin et al. [5]	Pyrolysis carbon replaces 5–20% of cement in mortar	Powder substitution in mortar	Closest cement-replacement comparison. The present work adds lower dosages and masonry bond.
Zhao et al. [6]	Recovered off-the-road tyre carbon as an aggregate constituent	Thermal-insulation mortar	A different constituent and target function govern selection.
Karthikeyan and Elavenil [10]	Processed tyre-derived pyrolytic carbon in mortar	Ultrasonication and superplasticiser-assisted dispersion	Dispersion conditions differ from mixing without dispersing admixtures.
Present study	0, 2.5, 5.0 and 7.5% cement replacement	Dried and sieved WTCB, no dispersing admixture	Paired bulk and masonry criteria identify bond loss despite favourable selected strength means.

3. Discussion

3.1. Fresh Mortar Consistency

With sand and effective water held constant, flow decreased from 113.06% to 105.94% as WTCB replacement increased from 0 to 7.5% (Table 1). Flow measures the percentage increase in spread diameter. The four readings at each dosage came from one spread, so they describe consistency within a single test. Water uptake in the adapted absorption test was 7.52% of the oven-dry powder mass (Table S15). This is consistent with greater wetting demand, although the absorption test does not measure the water taken up during mixing. Agglomeration may also restrict spread in the absence of a dispersant [8,10,13]. To test whether dispersion improves flow, independently mixed batches could be compared at the same effective water-to-total-powder ratio, with and without a dispersant, including corresponding controls without WTCB.

3.2. Compressive Strength and Nominal Diagonal Shear

At 5.0% replacement, the 28-day mean compressive strength exceeded the control by 0.763 MPa. The unadjusted 95% Welch interval ranged from −2.613 to +4.138 MPa (Table S9). The three loaded areas in this group were 26.8–27.7% below the nominal cube face (Table S8), and dosage and batch were inseparable. These constraints limit interpretation of the apparent maximum. Replacing cement increased the effective water-to-cement ratio at constant total powder mass (Table 8). Particle packing or hydrate nucleation might partly offset cement dilution [7,9], but the available records do not establish either mechanism. Independent batches and a second measurement of each loaded face before testing would help establish whether the ranking is reproducible.

Masonry compression and diagonal loading involve both the mortar and the units [11]. The 2.5% mixture had the highest mean prism strength on each test date (Table S16). At 28 days, its nominal diagonal shear strength exceeded the control by 0.034 MPa (95% interval, −0.002 to +0.071 MPa), while its crossed-brick tensile bond strength fell by 0.098 MPa (95% interval for the difference, −0.152 to −0.045 MPa). At 5.0% and 7.5%, the mean nominal diagonal shear strength was 7.39% and 16.41% below the control, respectively. Diagonal compression loads the whole panel, whereas the crossed-brick test pulls a single

joint apart. Peak loads alone cannot identify the failure path. Measuring brick moisture at laying and recording crack paths and joint contact in replicate panels and bond specimens would help identify what limits each response.

3.3. Flexural and Direct Tensile Strength

The 7.5% mixture had the highest mean flexural strength at 7 days, but the control ranked highest at 14 and 28 days (Table 2). At 28 days, the flexural means at 2.5%, 5.0% and 7.5% were 7.46%, 2.67% and 5.68% below the control, respectively. Each conditional 95% interval for the difference included zero (Table S9). The dosage–age interaction captures the change in ranking across ages and does not establish a strength loss at each dosage at 28 days. At 7.5%, mean direct tensile strength exceeded the control by 27.94% at 28 days. A beam develops a stress gradient in bending, whereas a briquette is loaded in axial tension. The two tests therefore need not rank mixtures in the same order.

Mahmood et al. [14] examined fracture behaviour in mortars containing dispersed pyrolytic particles as additions. Here, the particles displaced cement. Local agglomerates or voids on the tensile side of a beam could favour crack initiation, but the available measurements do not identify the initiation sites. A controlled comparison of dispersion methods should retain the same water content, span and beam geometry and document the fracture origin in each tested beam.

3.4. Application Limits and Material Qualification

Dosage selection must reflect the intended mortar–unit system. Among the modified mixtures, 2.5% retained the most flow and gave the highest prism and nominal diagonal shear means, whereas 7.5% incorporated more WTCB and had the smallest bond reduction. These outcomes require consideration of bond alongside compressive and flexural response, with acceptance limits defined for the intended units, joints and loading conditions [12].

The WTCB contained 25,788.97 mg kg^{-1} of total zinc (Table S10). Bowles et al. [15] observed changes in zinc sulphide diffraction peaks during demineralisation of a different recovered tyre carbon. Total zinc in the present powder does not establish its chemical form or its release from cured mortar.

Environmental evaluation requires a process inventory and a functionally equivalent masonry product. Maga et al. showed that the environmental balance of tyre pyrolysis depends on process inventories and the products displaced by recovered outputs [16]. A comparison for masonry should account for tyre collection, pyrolysis energy demand, recovered-carbon yield per unit of tyre feedstock, conditioning, transport, allocation of impacts among coproducts and service performance. The measured bond and strength responses provide performance criteria for selecting formulations for that assessment.

The measured sulphur and trace-element contents provide a basis for selecting analytes in exposure-specific leaching tests of cured mortar.

The comparisons apply to one WTCB source and one batch per dosage in each test series. Durability, leaching and life-cycle assessment should target formulations meeting the intended performance requirements. The present programme covers static specimen-scale tests. Full-wall, seismic and structural-code qualification require separate assessment.

4. Materials and Methods

4.1. Materials and WTCB Characterisation

We used Type I Portland cement, natural fine aggregate from the Pátapo–La Victoria quarry in Chiclayo, Peru, potable water and WTCB from end-of-life tyre pyrolysis. The specifications for cement and aggregate cited NTP 334.009 and NTP 400.037, respectively. The sand had a density of 2.245 g cm^{-3}, absorption of 4.59%, moisture content of 0.50% and

fineness modulus of 2.47. Sieve analysis followed NTP 400.012, and density/absorption testing followed NTP 400.022. The dry loose and compacted bulk densities were 1495.83 and 1657.28 kg m^{-3}, respectively. Tables S11 and S14 give the sand grading and the loose and compacted bulk densities on both moisture bases. No surfactant, superplasticiser or other chemical dispersant was added.

The tyre feedstock underwent steel and textile removal, shredding and oxygen-excluded pyrolysis at 350 °C for 120 min. The recovered solid cooled in a closed container before magnetic separation and milling. We dried the powder at 105 °C for 24 h, cooled it in a desiccator, passed it through a No. 200 sieve (75 µm) and stored it in a sealed container under dry conditions at 23 °C. The 75 µm sieve aperture defines the preparation cut-off. The WTCB density was 2.088 g cm^{-3}, determined by liquid displacement in a Le Chatelier flask with kerosene at 20 °C under the recorded NTP 334.005 procedure. The measured densities of the cement–WTCB powder blends were 2.053, 2.035 and 2.022 g cm^{-3} at 2.5%, 5.0% and 7.5% replacement, respectively (Table S14). The WTCB water absorption was 7.52% across two determinations, 7.56% and 7.49%, using the NTP 400.022 procedure adapted to the powder (Table S15).

The laboratory-reported elemental composition is given in Table 7. The report identified ASTM D5373 and ASTM D4239 for elemental analysis and ICP-OES for the screening panel. Carbon was 73.48%, and the ICP-OES zinc concentration was 25,788.97 mg kg^{-1}. Table S10 provides the complete ICP-OES screening results, retaining the analyte labels and method quantification limits reported by the laboratory.

Table 7. Reported elemental composition of waste tyre carbon black (WTCB).

Element	Content (%)	Limit of Quantification (%)
Carbon	73.48	0.01
Hydrogen	1.80	0.01
Oxygen	20.87	0.01
Nitrogen	0.32	0.01
Sulphur	3.53	0.01

Elemental results and method quantification limits follow laboratory report IE-2024-1198-02. LCM in the source denotes the method quantification limit. The report did not specify the elemental oxygen determination basis. Table S10 provides the separate ICP-OES dataset.

The aqueous-suspension pH was 6.86. For this determination, 10 g of WTCB was mixed with 100 mL of deionised water, gently boiled for 15 min and cooled to 25 °C. We recorded the stable value during gentle agitation with a combined glass electrode and temperature sensor after calibration at pH 4 and 7 at 25 °C. Our laboratory also measured the particle-size distribution, specific surface area, ash content and residual organics of the WTCB and examined its mineral phases by X-ray diffraction (XRD). Complementary testing also included scanning electron microscopy (SEM), thermogravimetric analysis (TGA) and derivative thermogravimetry (DTG), and hardened-mortar porosity. The laboratory did not issue a separate report for these eight tests. The Supplementary Materials do not include the individual readings, diffraction patterns, micrographs or thermal curves.

4.2. Mixture Preparation and Test Programme

We prepared four mixtures with WTCB replacing 0, 2.5, 5.0 or 7.5% of the reference cement mass. The 0–7.5% range covers replacement levels below and around the 5% level investigated in earlier mortar substitution work [5], at 2.5 percentage-point intervals. The original design designation was nominally 1:4, and Table 8 gives the actual reference masses and the corresponding replacement quantities. The reference cement charge was 357.14 kg per nominal cubic metre. WTCB displaced 8.93, 17.86 or 26.79 kg of this charge, so cement

plus WTCB remained 357.14 kg. The sum of cement and WTCB is termed total powder for mixture accounting. Sand and water were held constant across replacement levels.

Table 8. Mixture quantities on the reference design basis.

Constituent or Ratio	0%	2.5%	5.0%	7.5%
Cement (kg m^{-3})	357.14	348.21	339.28	330.35
WTCB (kg m^{-3})	0.00	8.93	17.86	26.79
Total powder (kg m^{-3})	357.14	357.14	357.14	357.14
Dry sand (kg m^{-3})	1415.34	1415.34	1415.34	1415.34
Moist sand (kg m^{-3})	1422.46	1422.46	1422.46	1422.46
Effective water (L m^{-3})	225.00	225.00	225.00	225.00
Introduced water (L m^{-3})	282.85	282.85	282.85	282.85
Effective water/total powder	0.6300	0.6300	0.6300	0.6300
Effective water/cement	0.6300	0.6462	0.6632	0.6811

Quantities are expressed per nominal cubic metre of the reference design, which assumes 3% air. Replacement-mixture masses follow the stated cement substitution rule, with sand and water unchanged. Dry and moist sand describe the same sand charge on two moisture bases. Introduced water includes the 57.85 L m^{-3} sand moisture/absorption adjustment.

The reference design specified 225 L m^{-3} of effective water. The sand absorption and moisture adjustment added 57.85 L m^{-3}, giving 282.85 L m^{-3} of water introduced during mixing and 1422.46 kg m^{-3} of moist sand (1415.34 kg m^{-3} dry). Thus, effective water/(cement + WTCB) was 0.63. Effective water/remaining cement increased from 0.6300 to 0.6462, 0.6632 and 0.6811 as replacement increased. The gross introduced-water/total-powder ratio was approximately 0.792 and is distinct from the effective ratio. Cement, WTCB and sand were mixed dry, followed by gradual water addition and mixing to a visually uniform consistency. Table 9 lists the tests, reference methods, test ages and numbers of specimens or flow readings.

Table 9. Test programme and method references.

Response	Method Reference	Age (Days)	Specimens
Mortar flow	NTP 334.057/ASTM C1437 [17]	Fresh	1 spread × 4 directions per dosage
Mortar compression	NTP 334.051:2013/ASTM C109/C109M [18]	7, 14, 28	3 × 4 × 3 = 36
Mortar flexure	NTP 334.120 [19]	7, 14, 28	3 × 4 × 3 = 36
Direct tensile strength	NTP 334.060:2019 [20]	7, 14, 28	3 × 4 × 3 = 36
Prism compression	NTP 399.605/ASTM C1314 [21]	28 (nominal)	6 × 4 = 24
Nominal diagonal shear	NTP 399.621/ASTM E519 [22]	14, 28	3 × 4 × 2 = 24
Mortar–unit bond	ASTM C952-12 (withdrawn) [23]	14, 28	3 × 4 × 2 = 24

Each mechanical test series comprised one mixing batch per dosage, giving 24 preparations for 180 specimens. Specimens within a dosage–test series shared a batch. Diagonal compression denotes the loading arrangement; nominal diagonal shear strength denotes the calculated response. Mortar–unit bond was measured in direct tension using crossed bricks.

Mortar compression used nominal 50 mm cubes, direct tension used briquettes, and flexure used 40 × 40 × 160 mm beams. We kept the moulded specimens at 23 °C and 95% relative humidity during the first 24 h, demoulded them at 24 h and immersed them in lime-saturated water at 23 °C until testing at 7, 14 or 28 days. The compression sheets cite NTP 334.051:2013 for nominal 50 mm mortar cubes. We used a load-control rate of 1200 N s^{-1}. Direct tension followed NTP 334.060:2019 [16], with axial tensile loading through the briquette grips at 45 N s^{-1}. Recorded reduced-section areas were 641 mm^2 for the control and 645 mm^2 for WTCB briquettes. The flexural records identified NTP 334.120 [15]. We

used central loading on two supports at 44 N s^{-1}, with the recorded support span of 130 mm. Flexural stress was calculated using the individual measured beam widths and depths.

We used solid fired-clay bricks of nominal dimensions 240 × 120 × 90 mm and 10 mm horizontal and vertical joints. The units were brush-cleaned and sprinkled for 30 min, ending 12 h before laying, leaving moist surfaces without free water. Prisms, diagonal panels and crossed-brick bond assemblies remained under cover at 23 °C and 70% relative humidity, with plastic protection during the first 48 h and no direct watering. The study protocol designated 28 days for prism compression [24]. The laboratory sheets give two test dates for each dosage, 5 and 19 October 2024, with three prisms on each date. They give no individual construction dates or curing ages. Panels and bond assemblies were tested at 14 and 28 days, with three specimens per dosage and age.

Prism compression followed the NTP 399.605 procedure identified in the laboratory sheets, using nominal 240 × 120 × 300 mm assemblages at 1.00 kN s^{-1}. Prism strength was calculated as 1.04 P/A, where P is peak load and A is the individual recorded bearing area. The laboratory adopted the factor 1.04 for the nominal height-to-thickness ratio of 2.5, consistent with the ASTM C1314 correction table [21]. Measured height-to-thickness ratios ranged from 2.42 to 2.55.

Diagonal panels measured approximately 0.63 × 0.63 m, with thicknesses of 120–125 mm. Steel shoes transferred the compressive load through opposite corners at 0.55 kN s^{-1} under the NTP 399.621 procedure identified in the laboratory sheets. Nominal diagonal shear strength was calculated as $v = 0.707\ P/A$, where P is peak load and A is the individual gross cross-sectional area. ASTM E519/E519M provides the diagonal tension (shear) framework [22]. Bond testing followed the crossed-brick direct-tension arrangement of the historical method ASTM C952-12, withdrawn in 2018 [23]. Two bricks formed a nominal 120 × 120 mm overlap with a 10 mm mortar joint. The assembly was loaded normal to the interface at 50 N s^{-1}, and tensile bond stress was calculated from peak load divided by the individual contact area. Table S6 gives all 24 peak loads and the contact areas reported to 0.001 m^2.

4.3. Data Processing and Statistical Analysis

The dataset comprises 180 specimens, with 36 each for mortar compression, direct tension and flexure and 24 each for prism compression, diagonal loading and bond. Each mortar strength test used three specimens per dosage at each of 7, 14 and 28 days. The diagonal shear and bond tests each used three specimens per dosage at both 14 and 28 days. Each prism dosage included three specimens per test date. Tables S1–S6 identify individual specimens by test, dosage and laboratory number. Table S5 identifies the fourth diagonal series by matching all six specimen records to the original study table [24].

Compression, direct tension, prism, nominal diagonal shear and bond summaries use the kgf cm^{-2} values printed on the laboratory sheets and the exact conversion 1 kgf cm^{-2} = 0.0980665 MPa. Flexural stress was recalculated from the recorded load, span and cross-sectional dimensions for central loading, as detailed in Section 4.4. We calculated arithmetic means and sample standard deviations from individual values before rounding. The original Pa and MPa columns remain available for traceability. For flow, four spread diameters measured in different directions were averaged within each test. Each dosage had one spread measurement with four directional readings. Flow was calculated as $100(D - D_0)/D_0$, using the mean spread D and the lower internal mould diameter D_0 = 98.21 mm recorded on the 2024 test sheet. A separate calliper check in 2026 gave 98.20, 98.22, 98.19 and 98.23 mm (mean 98.21 mm). Table S12 provides the spread readings and recalculation.

We used balanced two-factor analysis of variance (ANOVA) for dosage, age and their interaction in compression, direct tension, flexure, nominal diagonal shear and bond and a one-factor dosage model for the prism observations pooled over the two test dates. Table S7 reports sums of squares, degrees of freedom, F ratios and *p*-values, using specimen-level residual variation and a nominal significance threshold of 0.05. Each test–dosage series comprised one batch, so dosage and batch effects cannot be separated and the analysis is conditional on the tested preparations. The small cell sizes limited assessment of normality and equal variance. Interpretation therefore combines means, sample standard deviations and percentage changes. Table S9 reports differences from the control at 28 days for the age-labelled tests and across both test dates for prisms, with unadjusted 95% Welch intervals based on specimen variation. Table S16 gives the prism means for each date. These intervals exclude between-batch variability.

Supplementary association plots use dosage–age group means and Pearson correlations. Supplementary mean grids display the observed group mean at each tested dosage–age combination. The cell colours and numeric labels represent these measured means. We plotted the figures using Matplotlib 3.10.8.

4.4. Verification of Calculations and Data Definitions

The original compression sheets record individual loaded areas. For the three 5.0% WTCB cubes tested at 28 days, loads of 24,050, 24,820 and 24,090 N and areas of 1829, 1807 and 1825 mm^2 give 13.149, 13.735 and 13.200 MPa, respectively. These areas are 26.8–27.7% below the nominal cube face of 2500 mm^2. The other 33 recorded areas ranged from 2419 to 2636 mm^2. The 5.0% mean at 28 days therefore depends on these three smaller recorded areas. Table S8 documents the load–area calculation.

Flexural stresses were recalculated for the confirmed central three-point loading arrangement. The original tabulated strengths correspond closely to $PL/(bh^2)$, whereas a central point load requires $f = 3PL/(2bh^2)$, where P is peak load, L is the support span, b is the measured width and h is the measured depth. We therefore recalculated all 36 flexural stresses from the original loads and dimensions, with L = 130 mm. For example, P = 1028.72 N, b = 42.82 mm and h = 41.65 mm give 2.701 MPa. Table S3 gives the laboratory-reported loads and stresses alongside the recalculated strengths, and Table S13 provides the complete geometric calculation. The flexural strength summaries, ANOVA, confidence intervals and figures use the recalculated values.

5. Conclusions

Waste tyre carbon black produced different dosage rankings across mortar and masonry responses. Flow declined from 113.06% for the control to 105.94% at 7.5% replacement. At 28 days, the 5.0% mixture had the highest mean mortar compressive strength (13.364 MPa), while the 7.5% mixture had the highest mean direct tensile strength (2.038 MPa). Every modified mixture had lower flexural and mortar–unit bond means than the control, with bond reductions of 17.5–46.2%.

The 2.5% mixture ranked highest in prism compression on each recorded test date and in nominal diagonal shear at 28 days. It also had the greatest 28-day bond reduction. No replacement level improved all measured criteria. These contrasting rankings identify interfacial bond as an additional criterion alongside bulk mortar strength. Further qualification of low WTCB replacement levels should combine independent-batch replication with application-specific bond requirements.

Supplementary Materials: The following supporting information can be downloaded at https://www.mdpi.com/article/10.3390/recycling11120216/s1. Tables S1–S6 present individual records

for mortar compression, direct tension, flexure, prism compression, diagonal shear and mortar–unit bond, respectively. Table S7 reports specimen-level ANOVA. Table S8 verifies the 28-day compressive strengths at 5.0% WTCB using measured loaded areas. Table S9 reports differences from the control with conditional 95% confidence intervals. Tables S10–S13 provide the ICP-OES screening results and quantification limits, fine-aggregate grading, flow measurements and flexural-test calculations, respectively. Table S14 reports sand bulk density and moisture, and WTCB and blended-powder densities. Table S15 reports WTCB water absorption. Table S16 reports prism strengths by test date and replacement level. Figures S1–S3 cover mortar compression, Figures S4–S6 direct tension, Figures S7–S9 flexure, Figures S10–S12 nominal diagonal shear and Figures S13–S15 mortar–unit bond. Each set presents specimen distributions, group-mean associations and observed means.

Author Contributions: All five authors, A.M.T.-V., D.A.P.-T., J.L.L.-P., H.A.A.-R. and W.M.H.-A., contributed equally to conceptualisation, methodology, validation, formal analysis, investigation, resources, data curation, writing (original draft), writing (review and editing), visualisation, supervision and project administration. All authors have read and agreed to the published version of the manuscript.

Funding: Universidad Tecnológica del Perú funded the study and the article processing charge through institutional support without a grant number.

Data Availability Statement: The original contributions presented in this study are included in the article and its Supplementary Materials, including records for all 180 mechanical-test specimens. The Supplementary Materials do not include individual readings or instrument outputs for the eight complementary characterisation tests described in Section 4.1. Further inquiries can be directed to the corresponding author.

Conflicts of Interest: The authors declare no conflicts of interest. The funder had no role in the design of the study, the collection, analysis or interpretation of data, the writing of the manuscript or the decision to publish the results.

Abbreviations

ANOVA	Analysis of variance
ICP-OES	Inductively coupled plasma optical emission spectrometry
DTG	Derivative thermogravimetry
SEM	Scanning electron microscopy
TGA	Thermogravimetric analysis
WTCB	Waste tyre carbon black
XRD	X-ray diffraction

References

1. International Energy Agency. Cement and Concrete. In *Breakthrough Agenda Report 2025*; International Energy Agency: Paris, France, 2025. Available online: https://www.iea.org/reports/breakthrough-agenda-report-2025/cement-and-concrete (accessed on 19 October 2026).
2. Ministerio del Ambiente. *Decreto Supremo N.° 024-2021-MINAM: Régimen Especial de Gestión y Manejo de Neumáticos Fuera de Uso*; Ministerio del Ambiente: Lima, Peru, 2021. Available online: https://www.gob.pe/institucion/minam/normas-legales/2039546-024-2021-minam (accessed on 19 October 2026).
3. Rikmann, E.; Mäeorg, U.; Liiv, J. Recycling of Low-Quality Carbon Black Produced by Tire Pyrolysis. *Appl. Sci.* **2024**, *14*, 2192. [CrossRef]
4. Abdulfattah, O.; Alsurakji, I.H.; El-Qanni, A.; Samaneh, M.; Najjar, M.; Abdallah, R.; Assaf, I. Experimental evaluation of using pyrolyzed carbon black derived from waste tires as additive towards sustainable concrete. *Case Stud. Constr. Mater.* **2022**, *16*, e00938. [CrossRef]
5. Sabrin, R.; Shahjalal, M.; Bachu, H.A.E.; Habib, M.M.L.; Jerin, T.; Billah, A.H.M.M. Recycling of different industrial wastes as supplement of cement for sustainable production of mortar. *J. Build. Eng.* **2024**, *86*, 108765. [CrossRef]
6. Zhao, J.; Huang, G.; Guo, Y.; Gupta, R.; Liu, W.V. Developing thermal insulation cement-based mortars using recycled carbon black derived from scrapped off-the-road tires. *Constr. Build. Mater.* **2023**, *393*, 132043. [CrossRef]

7. Brial, V.; Duplessis, T.; Ouellet-Plamondon, C.M. Accelerating effect of low replacements of carbonaceous materials in cement paste and mortar. *CEMENT* **2024**, *18*, 100118. [CrossRef]
8. Zhang, J.; Qi, Y.; Lv, T.; Niu, X.; Tai, B. Effects of sodium dodecyl sulfate on nano carbon black-filled cement paste: Performance and microstructure. *J. Mater. Res. Technol.* **2023**, *24*, 1706–1715. [CrossRef]
9. de Lima, G.E.S.; Nalon, G.H.; Santos, R.F.; Ribeiro, J.C.L.; de Carvalho, J.M.F.; Pedroti, L.G.; de Araújo, E.N.D. Microstructural Investigation of the Effects of Carbon Black Nanoparticles on Hydration Mechanisms, Mechanical and Piezoresistive Properties of Cement Mortars. *Mater. Res.* **2021**, *24*, e20200539. [CrossRef]
10. Karthikeyan, N.K.; Elavenil, S. Dispersion effect of nano-structure pyrolytic carbon on mechanical, electrical, and microstructural characteristics of cement mortar composite. *Int. J. Smart Nano Mater.* **2024**, *15*, 534–578. [CrossRef]
11. Nalon, G.H.; Santos, C.F.R.; Pedroti, L.G.; Ribeiro, J.C.L.; Veríssimo, G.S.; Ferreira, F.A. Strength and failure mechanisms of masonry prisms under compression, flexure and shear: Components' mechanical properties as design constraints. *J. Build. Eng.* **2020**, *28*, 101038. [CrossRef]
12. Ministerio de Vivienda, Construcción y Saneamiento. *Norma Técnica E.070: Albañilería. Reglamento Nacional de Edificaciones*; Ministerio de Vivienda, Construcción y Saneamiento: Lima, Peru, 2006. Available online: https://www.gob.pe/institucion/vivienda/informes-publicaciones/2309793-reglamento-nacional-de-edificaciones-rne (accessed on 19 October 2026).
13. Wu, J.; Xie, S.; Ji, Z.; Wu, Z.; Ma, C.; Wang, J. Effect of nano carbon black content and dispersibility on the properties of cement paste. *Proc. Inst. Civ. Eng. Transp.* **2025**, *178*, 217–229. [CrossRef]
14. Mahmood, A.; Khushnood, R.A.; Zeeshan, M. Pyrolytic carbonaceous reinforcements for enhanced electromagnetic and fracture response of cementitious composites. *J. Clean. Prod.* **2020**, *248*, 119288. [CrossRef]
15. Bowles, A.J.; Wilson, A.L.; Fowler, G.D. Synergistic benefits of recovered carbon black demineralisation for tyre recycling. *Resour. Conserv. Recycl.* **2023**, *198*, 107124. [CrossRef]
16. Maga, D.; Aryan, V.; Blömer, J. A comparative life cycle assessment of tyre recycling using pyrolysis compared to conventional end-of-life pathways. *Resour. Conserv. Recycl.* **2023**, *199*, 107255. [CrossRef]
17. *ASTM C1437-20*; Standard Test Method for Flow of Hydraulic Cement Mortar. ASTM International: West Conshohocken, PA, USA, 2020. Available online: https://store.astm.org/c1437-20.html (accessed on 19 October 2026).
18. *ASTM C109/C109M-21*; Standard Test Method for Compressive Strength of Hydraulic Cement Mortars (Using 2-in. or [50 mm] Cube Specimens). ASTM International: West Conshohocken, PA, USA, 2021. Available online: https://store.astm.org/c0109_c0109m-21.html (accessed on 19 October 2026).
19. *NTP 334.120:2023*; Cementos. Método de Ensayo Normalizado de Resistencia a la Flexión de Mortero de Cemento Hidráulico, 3rd ed. Instituto Nacional de Calidad (INACAL): Lima, Peru, 2023.
20. *NTP 334.060:2019*; Cementos. Método de Ensayo Para Determinar la Resistencia a la Tensión de Morteros de Cemento Hidráulico, 2nd ed. Instituto Nacional de Calidad (INACAL): Lima, Peru, 2019.
21. *ASTM C1314-23a*; Standard Test Method for Compressive Strength of Masonry Prisms. ASTM International: West Conshohocken, PA, USA, 2023. Available online: https://store.astm.org/c1314-23a.html (accessed on 19 October 2026).
22. *ASTM E519/E519M-22*; Standard Test Method for Diagonal Tension (Shear) in Masonry Assemblages. ASTM International: West Conshohocken, PA, USA, 2022. Available online: https://store.astm.org/e0519_e0519m-22.html (accessed on 19 October 2026).
23. *ASTM C952-12*; Standard Test Method for Bond Strength of Mortar to Masonry Units (Withdrawn 2018). ASTM International: West Conshohocken, PA, USA, 2012. Available online: https://store.astm.org/c0952-12.html (accessed on 20 October 2026).
24. Pacheco Torres, D.A.; Torres Vásquez, A.M. Evaluación de las Propiedades Físico-Mecánicas del Mortero Sustituyendo Parcialmente el Cemento por Negro de Humo de Neumáticos, Chiclayo-2024. Bachelor's Thesis, Universidad Tecnológica del Perú, Chiclayo, Peru, 2025.

Disclaimer/Publisher's Note: The statements, opinions and data contained in all publications are solely those of the individual author(s) and contributor(s) and not of MDPI and/or the editor(s). MDPI and/or the editor(s) disclaim responsibility for any injury to people or property resulting from any ideas, methods, instructions or products referred to in the content.